# Numerical Assessment of Passive Decay Heat Removal in a Molten Salt Reactor Drain Tank

KyongDong Im[a], Hoon Chae[a], Nam-il Tak[b], Eung Soo Kim [a*]
[a]*Department of Nuclear Engineering, Seoul National University, 1 Gwanak-ro, Gwanak-gu, Seoul*
[b]*Korea Atomic Energy Research Institute, 111 Daedeok-daero 989beon-gil, Yuseong, Daejeon, Korea*
[*]*Corresponding author: kes7741@snu.ac.kr*

***Keywords : Molten salt reactor, Drain tank, Passive decay heat removal, Conjugate heat transfer, CFD**

## 1. Introduction

Passive decay heat removal is a key safety function for Molten Salt Reactors (MSRs), especially under station blackout conditions where external power is unavailable. In contemporary MSR designs, integrating an emergency drain tank is a widely considered approach to safely managing the molten salt during shutdown or accident scenarios [1, 2]. However, for a compact reactor platform, the limited space significantly constrains the feasible passive cooling concepts, potentially raising licensing concerns regarding the reliability of natural heat dissipation. When MSR is shutdown, decay heat generated in the drained fuel salt must be reliably removed through passive pathways to prevent excessive temperatures in the drain tank and surrounding structures [3].

To ensure the structural integrity and safety of the system, it is imperative to comprehensively understand the thermal behavior of the passive cooling mechanisms. This work performs a 3D CFD-based conjugate heat transfer analysis—conduction, natural convection, and thermal radiation—for an MSR drain-tank passive cooling scenario. The primary contributions of this study include the establishment of a rigorous numerical model confirmed by grid-independence tests, a detailed parametric sensitivity analysis using normalized indicators, and the identification of dominant cooling mechanisms through heat-transfer partitioning.

## 2. Modeling and numerical methods

### *2.1. Geometry and domain*

The computational domain encompasses the drain tank, containment, internal structure (including H-beams), and the surrounding air region. To accurately capture the natural circulation of the surrounding air and the complex heat pathways, the conjugate heat transfer domain was fully modeled.

### *2.2. Physics Models*

The thermal fluid behavior is resolved using Ansys Fluent, incorporating a coupled conjugate heat transfer approach. The Shear-Stress Transport (SST) $k-\omega$ model is employed to predict the natural convection and turbulent flow of the air [4]. For surface radiation, the Surface-to-Surface (S2S) radiation model is utilized. The S2S model is highly suitable for this application since the intervening air medium is assumed to be non-participating (i.e., ignoring absorption and scattering), and all solid surfaces are treated as gray-diffuse bodies characterized by their respective view factors. Buoyancy-driven flow was modeled with gravity enabled, and density variation of air was treated using the Boussinesq approximation with a reference temperature $T_{\infty,ref}$.

### *2.3. Boundary and initial conditions*

The internal heat generation, representing the decay heat of the drained molten salt, is applied to the interior volume of the drain tank and is defined in a normalized form as $Q^* = Q/Q_{ref}$. The external boundary of the containment exchanges heat with the ambient environment at temperature of 298.15K, characterized by a normalized external heat transfer coefficient, $h^* = h/h_{ref}$. The bottom surface of the domain is assumed to be adiabatic, implying no heat loss to the ground. Surface emissivities ($\varepsilon$) are assigned to the drain tank and containment walls, and variations of these values are evaluated in the sensitivity study. All simulations were conducted under steady-state assumptions, representing quasi-steady snapshots at specified decay-heat levels. This approach allows a conservative assessment of equilibrium peak temperatures and enables an isolated comparison of boundary-condition sensitivities.

**Table. I Parameter ranges and baseline conditions for the sensitivity analysis.**

| Parameter | Range | Baseline (reference case) |
|---|---|---|
| $T_\infty$ | $-40 \sim 38^\circ C$ | $25^\circ C$ |
| $h^*$ | 1 ~ 4 | 1 |
| $\varepsilon_{container}$ | 0.2 ~ 0.8 | 0.2 |
| $\varepsilon_{draintank}$ | 0.2 ~ 0.8 | 0.3 |

### *2.4. Data post-processing and normalization scheme*

Temperature data is normalized based on the temperature rise relative to the ambient condition:

$$\Delta T = T - T_\infty, \qquad \Delta T^* = \frac{\Delta T}{\Delta T_{ref}} \tag{1}$$

This normalization effectively shows the relative trends among parameters. Furthermore, the contributions of individual heat transfer modes are evaluated using fraction ratios:

$$f_{rad} = \frac{Q_{rad}}{Q_{total}}, \quad f_{conv} = \frac{Q_{conv}}{Q_{total}}, \quad f_{cond} = \frac{Q_{cond}}{Q_{total}} \quad (2)$$

Convergence was declared when residuals for momentum and energy dropped below a 1E-3 and the global heat imbalance was within an 1E-6.

## 3. Results and discussion

### *3.1. Grid independence*

A grid independence study was conducted to ensure spatial convergence, using three mesh levels: coarse, normal, and fine as detailed in Table. II. The normalized peak temperature ($\Delta T^*_{max}$) of the drain tank was compared across the different mesh models as shown in Fig. 1. The results show that while the coarse mesh underpredicts the peak temperature, the variation in $\Delta T^*_{max}$ became negligible between the normal and fine mesh configurations, indicating asymptotic convergence. A similar convergence trend was also observed for the containment peak temperature. Consequently, the normal mesh was adopted for all subsequent parametric studies to achieve an optimal balance between computational efficiency and accuracy.

**Table. II. Mesh parameters for grid independence.**

| | Coarse mesh | Normal mesh | Fine mesh |
|---|---|---|---|
| Number of Cells [#] | 2,527,826 | 3,680,768 | 10,250,828 |
| Max cell size [m] | 0.1 | 0.05 | 0.03 |
| Mesh type | tetrahedral | tetrahedral | tetrahedral |

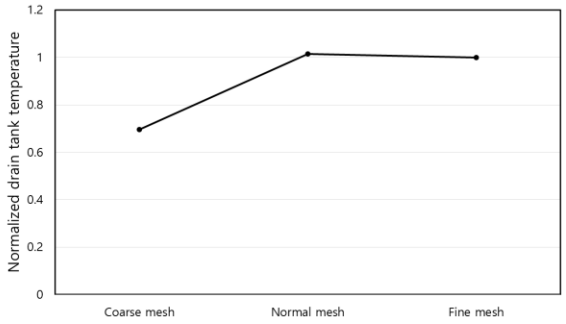


**Fig. 1 Normalized peak temperature of drain tank across different mesh resolutions.**

### *3.2. Sensitivity to heat-transfer parameters*

A parametric sensitivity study was performed by varying key heat-transfer parameters around the baseline case : ambient temperature $T_\infty$, normalized external heat transfer coefficient $h^*$, containment emissivity $\varepsilon_{container}$, and drain-tank emissivity $\varepsilon_{draintank}$. Fig. 2 summarizes the sensitivity trends for each parameter.

First, varying the ambient temperature from $-40°C$ to $38°C$ led to moderate changes in the normalized peak temperatures, with $\Delta T^*$ ranging from 0.991 to 1.096 for the drain tank and from 0.984 to 1.127 for the containment (Fig. 2(a)). Since the metric is normalized based on the temperature rise relative to the ambient condition, a colder ambient can yield a larger normalized temperature rise, while the present discussion focuses on relative trends rather than absolute values.

The containment temperature is most strongly governed by the external heat rejection condition. As $h^*$ increases from 1 to 4, the containment $\Delta T^*$ decreases significantly from 1.000 to 0.604, whereas the drain-tank $\Delta T^*$ exhibits only a weak dependence (0.942–1.000) (Fig. 2(b)). This indicates that the containment wall temperature is primarily controlled by the external convection boundary, while the drain-tank peak is comparatively less sensitive once radiative heat transfer to the enclosure is established.

The containment emissivity also shows a pronounced effect. Increasing $\varepsilon_{container}$ from 0.2 to 0.8 reduces the containment $\Delta T^*$ from 1.026 to 0.853 (approximately 15% reduction), and the drain-tank $\Delta T^*$ from 1.028 to 0.948 (approximately 5% reduction) (Fig. 2(c)). A higher $\varepsilon_{container}$ enhances radiative heat loss from the containment surfaces to the ambient, lowering the overall temperature level of the enclosure.

In contrast, the drain-tank emissivity dominantly affects the drain-tank temperature. Increasing $\varepsilon_{draintank}$ from 0.2 to 0.8 decreases the drain-tank $\Delta T^*$ from 1.000 to 0.798 (approximately 20% reduction) (Fig. 2(d)). Meanwhile, the containment $\Delta T^*$ slightly increases up to 1.071, which is consistent with enhanced radiative heat exchange from the drain tank to the containment. Overall, the drain-tank peak is most sensitive to $\varepsilon_{draintank}$, whereas the containment peak is primarily governed by $h^*$ and $\varepsilon_{container}$, indicating that surface radiative properties and external heat rejection conditions are the key uncertainty drivers.

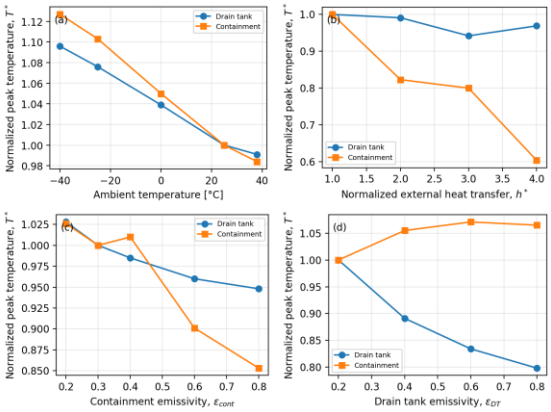


**Fig. 2. Sensitivity of normalized peak temperatures to key heat-transfer parameters: (a) ambient temperature, (b) normalized external heat transfer coefficient, (c) containment emissivity, and (d) drain-tank emissivity.**

### *3.3. Heat transfer partitioning*

The total decay heat removed from the system was decomposed into radiation, convection, and conduction fraction ($f_{rad}$, $f_{conv}$, and $f_{cond}$) to identify the dominant cooling mechanisms. Here, $Q_{rad}$, $Q_{conv}$, and $Q_{cond}$ denote the net heat transfer components leaving the drain-tank surface, evaluated by surface-integrated radiative, convective, and conductive heat fluxes, respectively. The analysis indicates a strong dependency on the normalized decay heat level ($Q^*$). As $Q^*$ increases, driving the system to higher absolute temperatures, the radiative fraction ($f_{rad}$) becomes distinctly dominant due to the $T^4$ dependence of thermal radiation. Conversely, as $Q^*$ decreases, the relative contributions of natural convection and conduction through the support structures progressively increase.

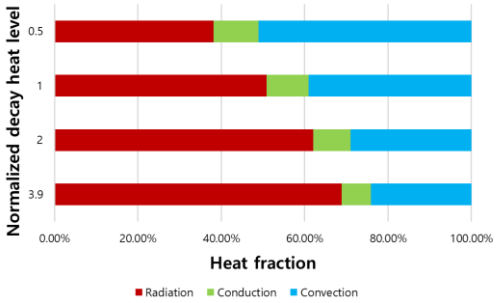


**Fig. 3. Heat transfer partitioning fraction**

## 4. Conclusions

A 3D conjugate heat transfer analysis for the passive cooling of an MSR drain tank was successfully performed, adhering to strict normalization protocols for confidentiality. Grid independence was confirmed, and the governing physical models robustly captured the complex interactions of conduction, convection, and radiation. The sensitivity assessment demonstrated that the drain tank's peak temperature is highly governed by surface emissivity, while the containment is more susceptible to external heat transfer coefficients. Furthermore, heat-transfer partitioning highlighted that radiation acts as the dominant heat removal mechanism at elevated decay heat levels. Further studies including experimental/benchmark validation and transient analyses are warranted to reduce uncertainties and extend the present steady-state assessment.

## ACKNOWLEDGEMENT

This work was supported by Korea Research Institute for defense Technology planning and advancement(KRIT) Grant funded by Defense Acquisition Program Administration(DAPA)(KRIT-CT-22-017, Next Generation Multi-Purpose High Power Generation Technology (Liquid Fueled Heat Supply Module Design Technology), 2022).

## REFERENCES

[1] Péniguel, C. "Thermal study of the emergency draining tank of molten salt reactor." *Nuclear Engineering and Technology* 56.3 (2024): 793-802.
[2] Wang, Shisheng, et al. "A passive decay heat removal system for emergency draining tanks of molten salt reactors." *Nuclear Engineering and Design* 341 (2019): 423-431.
[3] Parsly, L. F. MSRE Drain Tank-Heat Removal Studies. No. CF--60-9-55. Oak Ridge National Laboratory (ORNL), Oak Ridge, TN (United States), 1960.
[4] Menter, Florian R. "Two-equation eddy-viscosity turbulence models for engineering applications." *AIAA journal* 32.8 (1994): 1598-1605.